Long-range ground deformation measurement using interferometric synthetic aperture radar data on both up-going and down-going orbits

Shuichi Rokugawa
The University of Tokyo
Hongo7-3-1,Bunkyo-ku,Tokyo,Japan
rokugawa@ gpl.t.u-tokyo.ac.jp

Takako Nakamura
The University of Tokyo
Hongo7-3-1,Bunkyo-ku,Tokyo,Japan
nakamura@geosys.t.u-tokyo.ac.jp

Jun Matsushima
The University of Tokyo
Hongo7-3-1,Bunkyo-ku,Tokyo,Japan
jun-matsushima@frcer.t.u-tokyo.ac.jp

SUMMARY

Interferometric Synthetic Aperture Radar (InSAR) is a technique for mapping subtle surface deformations over a two-dimensional areas with high spatial resolution. The objective of this study is to evaluate the capability of InSAR analysis using both up-going and down-going orbits data for monitoring the long-range ground deformation caused by the environmental disaster. Differential InSAR (DInSAR) analysis and InSAR time series analysis were performed around disaster areas of the Kirishima Mountains in Japan (Fig. 1). The data used in this study were images from the Advanced Land Observation Satellite/Phased Array Synthetic Aperture Radar (ALOS/ PALSAR) observed from 2007 to 2011. We performed DInSAR analysis and InSAR time-series analysis with a commercial software and attempted to precisely estimate vertical and horizontal displacements by using the vector composition method from the observation data of both orbits. The results show that InSAR analysis is effective for the disaster monitoring of volcanic eruptions. Uplift and subsidence were detected around the Kirishima Mountains before the last eruption on January 26, 2011. This result suggests that long-range InSAR analysis has a capability to detect the symptoms of volcanic eruptions.

Key words: ALOS/PALSAR, InSAR, Kirishima Mountains, volcanic eruption, dual orbits.

INTRODUCTION

In this study, we performed the point-wise vector composition analysis of the target area by using the microwave remote sensing data from up-going and down-going orbits, and also attempted to estimate horizontal and vertical displacements with higher precision.

We applied the method of ground deformation measurement by combining InSAR and time-series analysis to the Kirishima volcano (Shin-Moedake) in Kyushu Island. Totally, 43 images of ALOS/PALSAR were used in this analysis. The land deformation is an unknown parameter in this method, and the smoothness-constrained inversion algorithm is applied to derive the deformation by the optimal solution.
The mechanisms of volcanic eruptions are not fully solved, and scientific prediction is difficult. However, the satellite based remote sensing can easily perform the long-range ground deformation monitoring, and also the detailed analysis of this deformation has a possibility to detect the subtle ground movements. We also examined whether InSAR could apply to the monitoring of associated eruption activities.

Figure 1. Index map of the study area.

METHOD

Typically, only the surface deformation along the radar direction from the satellite to the target can be obtained from InSAR observations. The true displacement vector of the ground surface is projected to the radar directions both in up-going and down-going orbits.

The essence of this problem is how to derive the true displacement vector from the scattering data in complex form acquired from these two orbits. The true displacement (vector **c** shown in Fig.2) is obtained by composition of two vectors (**a**, **b**) projected along radar directions as shown in the following numerical equations. The starting point of vector **c** is the observation point, and the terminal point of it can be determined by the intersection line of each plain perpendicular to vectors **a** or **b** and the plain defined by both vectors (Fig. 2). Finally the horizontal and vertical component of displacement (vector **c)** can be easily derived (Fig.2).

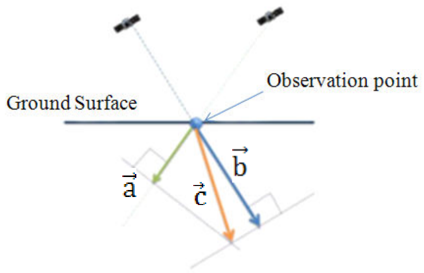

Figure 2. Vector composition based on data from two orbits.

The formulas for vector **c** are as follows.

$$\begin{cases} \mathbf{c} = \mathbf{k} * \mathbf{a} + \mathbf{l} * \mathbf{b} \\ \mathbf{a} \cdot (\mathbf{c} - \mathbf{a}) = 0 \\ \mathbf{b} \cdot (\mathbf{c} - \mathbf{b}) = 0 \end{cases}$$

The validity of this method was checked by the point-wise comparison of related images, such as two apparent displacement images along radar directions, horizontal and vertical component images. The varieties of displacement patterns were selected for this validation.

InSAR analysis system used here is the combination of commercial software and the original time-series analysis program. In addition, the dual orbit analysis system was originally developed. Quantitative evaluation of error factors in InSAR time-series analysis can be performed by simulating the SAR observations from two orbits. The seven factors that contribute to the error in InSAR measurement are summarized in Table 1. By evaluating the these errors, which influences the phase values, a practical data set yielding improved accuracy can be selected and processed.

Before the InSAR process, single-look complex (SLC) images including phase information were generated by the commercial software in the normal case. However PALSAR images were provided as single-look complex images. The SLC data sets of a target area were then precisely registered, and the interferometric images were calculated for all data pairs by considering the criteria shown in Table 1. The least-squares method based on the singular value decomposition was used in the inversion process. The following equation represents the principles of the inversion process.

$$S = \sum_{m=1}^{M} W\left\{\Delta\Phi_m - (t_l - t_k) - \frac{4\pi B_{perp}}{\lambda\rho \sin\alpha}\Delta h\right\}^2 + \mu^2 \sum_{n=1}^{N} (t_n - 2t_{n-1}t_{n-2})^2$$

B_{perp}: perpendicular component of spatial baseline

Δh: elevation error	*λ: wavelength*
ρ: slant range length	*W: Tukey's biweight function*
α: incidence angle	*μ^2: smoothing parameter (fixed to 1.0)*

Table 1. Quantitative evaluation of phase error factors.

	JERS-1/SAR	PALSAR (34.3/41.5)	ENVISAT/ASAR
1. Image Registration	± 0.2 pixels ξ_{calc}=0.96		
2. Baseline Estimation	Method of least squares		
3. Critical Baseline Calculation	$\gamma_{Bperp} = 1.0 - \frac{B_{perp}}{B_{critical}}$ $B_{critical} = \frac{\lambda\rho\tan\varphi}{2d_{rg}}$ (Theoretical calculation)		
4. Atmospheric effects	Seasonal variance of atmosphere		
5. Decrease in coherence	$TB_{critical}$= 1,399 (day) $B_{critical}$=1,703 (m)	$TB_{critical}$=1,400 $B_{critical}$=3,700/5,600 (m)	$TB_{critical}$=1,389 (day) $B_{critical}$=495 (m)
6. Sensor noise	ξ_{noise}=0.83	ξ_{noise}= 0.95	ξ_{noise}=0.95
7. DEM (precision of height)	$\Delta\phi_{\Delta h} = \frac{4\pi\Delta h}{\lambda\rho\sin\varphi} B_{perp}$ ⇒ select small baseline pairs		

$\gamma = \gamma_{calc} \times \gamma_{Bperp} \times \gamma_{temp} \times \gamma_{noise}$ $\Delta\phi_\gamma = \frac{1}{\sqrt{2N}}\sqrt{\frac{1-\gamma^2}{\gamma^2}}$ N number of multi-look, γ coherence, $\Delta\phi_\gamma$ Standard deviation of phase error (rad)

(Deguchi,2009)

RESULT AND DISCUSSION

The result of the time series analysis for both orbits around the Kirishima Mountains is shown in Fig. 3. The five image pairs show the features around January in 2007(top), 2008 (upper middle), 2009 (middle), 2010 (lower middle), and 2011 (bottom). Uplift is observed near the peaks of Mt. Karakuni and Takachihonomine in 2009, whereas subsidence is observed in 2010 and 2011.

The four-year ground deformation profiles from down-going orbit for Mt. Karakuni, Mt. Shinmoe, and Takachihonomine are shown in Fig. 4. The figure shows that the deformation trends for Mt. Karakuni and Takachihonomine changed from uplift to subsidence around 2009. Moreover, Mt. Shimmoedake first indicates the flat movement then subsided about 4cm/year, and exhibited a calm period of about one year before erupting on January 26, 2011.

In this study, the deformation direction for Mt. Shinmoedake was opposite to that for Mt. Karakuni or Takachihonomine. Interestingly, Mt. Shinmoedake began to subside rapidly and erupted shortly after Mt. Karakuni and Takachihonomine had uplifted to the maximum. The above-mentioned phenomena should reflect the geological structure and energy flow of the underground on the eve of the eruption.

Horizontal and vertical displacements were derived by vector composition analysis. Horizontal and vertical components are indicated as both **x** and **z** components of displacement vector. The spatial distribution maps of each component are shown in Fig.5. The processed image in the left panel shows the horizontal displacement along the EW direction. The colour transition from left to right in the colour bar indicates the movement toward right. In the right image, the similar colour transition indicates the uplift deformation also shown in the colour bar. This image suggests that the horizontal displacement was also remarkable compared with the vertical displacement shown in the right panel. This vector composition analysis indicates that the actual direction of displacement is very complicated around the volcanic area.

CONCLUSIONS

In the analysis of Kirishima Mountains, the vector composition analysis method using up-going and down-going orbit data derived more precise displacement vectors. The actual direction of displacement was clearly indicated by this

analysis. This result indicates the importance of dual orbit observation.
The prediction possibility of volcanic eruption was also shown by the long-range observation of surface displacements. The effectiveness of time-series analysis based on the least-square fitting scheme was clearly demonstrated.
In these case studies, some difficulties of analysis are also indicated. It remains difficult to register two images with different orbit because of the image distortion of radar images such as foreshortening or layover. Second difficulty is the less availability of down-going orbit data. ALOS has both optical and radar sensors, then down-going orbit is usually used for the data acquisition of optical sensors because of daytime flight. SAR is mainly operated as the nighttime observation in up-going orbit.
Finally, it should be noted that the action of the earth's surface is complicated, and then it is necessary to accumulate many case studies in various surface conditions.

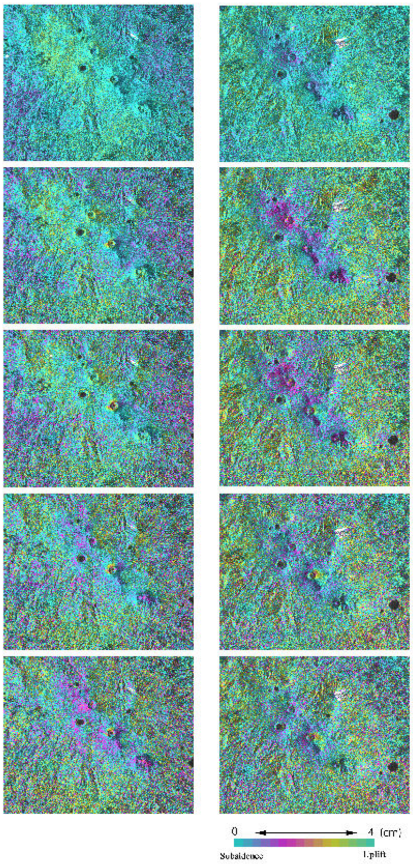

(Ascending: left, Descending: right)
Figure 3. Results of time-series analysis around the Kirishima Mountains

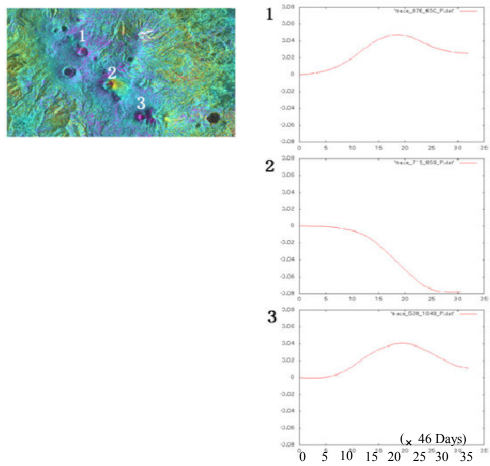

Figure 4. Temporal profile of estimated change at each mountain

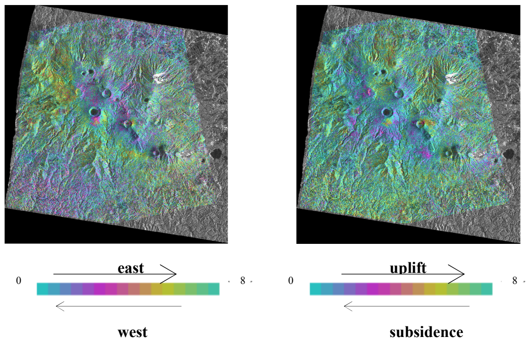

Figure 5. Vector composition of up-going and down-going orbits data. It shows the displacement value of the x (left), and z (right) directions.

ACKNOWLEDGMENTS

The authors would like to thank ERSDAC for providing PALSAR L band data.

REFERENCES

Deguchi, T., Rokugawa, S., and Matsushima, J., 2009, Long-term Ground Deformation Measurement by Time Series Analysis for SAR Interferometry: Journal of the Remote Sensing Society of Japan, **29**, 2, 418-428.

Ferretti, A., Prati, C., Rocca, F., 2000, Nonlinear Subsidence Rate Estimation Using Permanent Scatterers in Differential SAR Interferometry: IEEE Transactions on Geoscience and Remote Sensing, **38**, 5, 2202-2212.

Okuyama, S., 2009, Two-Dimensional Surface Displacement Associated with the M7.2 Iwate Miyagi Nairiku Earthquake, 2008 Detected by PALSAR Interferometry: Coordinating Committee for Earthquake Prediction Report, **81**,268-269

Rokugawa, S., 2010, The Surveillance Study about the Technical Subject for ALSAR Data Promotion of Utilization: Acceptance Research Report